Chemical Engineering Journal 333 (2018) 721–729

Contents lists available at ScienceDirect

Chemical Engineering Journal

journal homepage: www.elsevier.com/locate/cej

Electrosprayed $BiVO_4$ nanopillars coated with atomic-layer-deposited ZnO/TiO_2 as highly efficient photoanodes for solar water splitting

Min-Woo Kim[a,1], Karam Kim[a,1], Tae Yoon Ohm[a], Hyun Yoon[b], Bhavana Joshi[a], Edmund Samuel[a], Mark T. Swihart[c], Sung Kyu Choi[d], Hyunwoong Park[d], Sam S. Yoon[a,*]

[a] School of Mechanical Engineering, Korea University, Seoul 136-713, Republic of Korea
[b] KIER-UNIST Advanced Center for Energy, Korea Institute of Energy Research (KIER), 50, UNIST-gil, Ulsan 44919, Republic of Korea
[c] Department of Chemical & Biological Engineering, University at Buffalo, The State University of New York, Buffalo, NY 14260-4200, USA
[d] School of Energy Engineering, Kyungpook National University, Daegu 41566, Republic of Korea

GRAPHICAL ABSTRACT

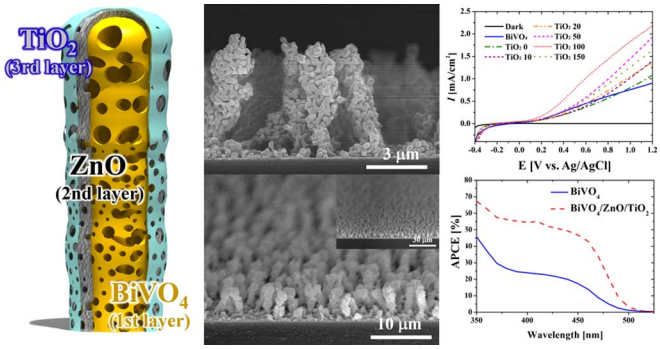

ARTICLE INFO

Keywords:
Bismuth vanadate nanopillar
Photoanode
Water splitting
Photocurrent density
Atomic layer deposition
Heterostructure

ABSTRACT

We report the fabrication and the performance in photoelectrochemical water splitting of thin films of electrostatically sprayed nanotextured bismuth vanadate ($BiVO_4$) pillars coated with thin ZnO/TiO_2 passivation layers formed by atomic layer deposition. The thin ZnO and TiO_2 layers deposited on the $BiVO_4$ nanopillars formed a heterostructure that promoted electron–hole separation and the migration of electrons toward the ITO substrate. The photocurrent density (PCD) of the ZnO/TiO_2 coated $BiVO_4$ was 2.5 times higher (2.25 mA/cm^2 at 1.2 V (versus Ag/AgCl)) than that of pristine $BiVO_4$ (0.9 mA/cm^2 at 1.2 V (versus Ag/AgCl)). We present incident/absorbed photon-to-current efficiency and electrochemical impedance measurements confirming that this improvement is a result of the heterojunction produced by the conformal ZnO/TiO_2 coating and discuss the mechanism of this dramatic enhancement of PCD.

1. Introduction

Starting from the first report of the photocatalytic decomposition of water (or photolysis) using TiO_2 by Fujishima and Honda in 1972, many semiconductor materials have been explored for use in solar water splitting [1]. The pioneering work of Fujishima was based on ultraviolet (UV) light. However, only a small fraction of the UV radiation from the sun reaches the earth, and most solar energy available at the earth's surface is at longer wavelengths. Harnessing the majority of the solar energy available for water

* Corresponding author.
E-mail address: skyoon@korea.ac.kr (S.S. Yoon).
[1] These authors have contributed equally.

http://dx.doi.org/10.1016/j.cej.2017.09.130
Received 18 July 2017; Received in revised form 20 September 2017; Accepted 22 September 2017
Available online 25 September 2017
1385-8947/

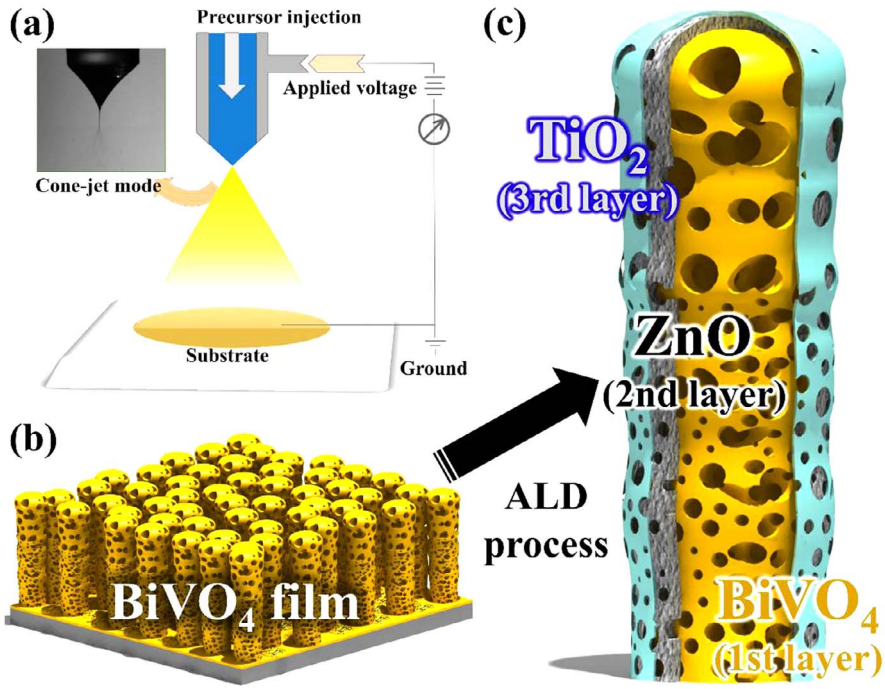

Fig. 1. Schematic of (a) electrostatic spray deposition process and (b) resulting $BiVO_4$ nanopillars and (c) ZnO/ TiO_2 layers formed over the nanopillars by ALD.

splitting requires semiconductors with a bandgap in the range of 1.6–3.2 eV.

Bismuth vanadate ($BiVO_4$) is an n-type semiconductor that occurs in tetragonal and monoclinic scheelite-like phases with bandgaps of 2.9 and 2.4 eV, respectively, and that has shown promise as a photoanode material [2–5]. The band structure of $BiVO_4$ involves the 3d orbitals of V, the 6s orbitals of Bi, and the 2p orbitals of O. The 6s orbitals of Bi are hybridized with the 2p orbitals of O to form hybrid valence bands, while the conduction band (CB) is comprised mainly of the 3d orbitals of V. This band structure promotes high mobility of the photogenerated carriers in $BiVO_4$, which supports high photocatalytic activity. However, the lifetimes of the photogenerated charge carriers in $BiVO_4$ are low, as they are able to recombine rapidly. Furthermore, the relatively short carrier-diffusion length in $BiVO_4$ results in poor charge migration and transfer properties [6]. Efforts to improve the photocatalytic activity of $BiVO_4$ by doping it with elements such as Mo and W have been reported [7,8]. Other methods such as using co-catalysts and forming heterojunction structures have also been explored for boosting the performance of $BiVO_4$ photoanodes [9,10].

The coupling of $BiVO_4$ with different oxides is a promising approach for improving the photoelectrochemical performance of $BiVO_4$. Introducing heterojunction layers that tune the position of its band gap increases its light-absorption range and improves the electron–hole pair-separation efficiency and the charge-transfer efficiency. A few examples of such materials are $BiVO_4/WO_3$, $BiVO_4/TiO_2$, and $BiVO_4$/ZnO [11–13].

TiO_2, which can be used as a photoanode material only in the UV range, has been studied extensively for use in water splitting applications. Scheuermann et al. [14] studied the effect of atomic layer deposition (ALD)-coated TiO_2 on the water oxidation performance of metal-insulator silicon anodes. They suggested that a thin layer of TiO_2 is sufficient for facilitating electron transport between the semiconductor absorber and the catalyst for the oxygen evolution reaction. Hu et al. formed a 143-nm-thick TiO_2 layer over a semiconductor (such as Si, GaAs, or GaP) as a passivation layer to minimize surface corrosion, which is a common problem during water oxidation [15].

ZnO has also been deposited on $BiVO_4$ to form a heterojunction layer that increases the photocurrent density. Further, it has been studied as a photocatalyst for dye degradation and self-cleaning [12,16,17]. Moniz et al. fabricated a ZnO/$BiVO_4$ structure over a fluorine-doped tin oxide substrate to form a water-splitting cell. The reduction performance of the cell improved after the formation of the ZnO/$BiVO_4$ heterostructure. In addition, charge transfer improved, which, in turn, increased the PCD of the cell [12]. Fu et al. [16] also reported an improvement in the photoelectrochemical (PEC) activity in a $BiVO_4$/ZnO structure; this was because ZnO prolonged the lifetime of the charge carriers and promoted electron–hole separation. Thus, the benefits of using heterostructured layers with $BiVO_4$ are evident [18].

Herein, we report the fabrication of a heterostructure consisting of electrostatic-spray-deposited (ESD) $BiVO_4$ nanopillars coated with ALD processed ZnO and TiO_2 layers, which enhanced the PCD. The ESD process produces extremely fine drops (less than a micron in size) with very uniform size distribution. These charged drops were attracted to the electrically grounded substrate. This provided very efficient deposition and eliminated precursor wastage, as all the charged drops were attracted to the substrate and adhered to it. The $BiVO_4$ drops initially produce a rough surface morphology. Subsequent drop deposition and adherence are concentrated at points of electric field concentration, which are the highest points in the layer. This further increases roughness and ultimately produces nanopillars. These nanopillars were then coated by ZnO and TiO layers using ALD. The effects of the addition of these layers, which produce an increase in the PCD, were then analyzed to optimize PEC performance.

2. Experimental procedure

2.1. Electrostatic spray deposition of $BiVO_4$ film

The precursor solution for the $BiVO_4$ nanopillars was prepared by mixing bismuth (III) nitrate pentahydrate ($BiN_3O_9{\cdot}5H_2O$, ≥98%, Sigma-Aldrich, 1.08 g), vanadium (III) acetylacetonate ($V(C_5H_7O_2)_3$, Sigma-Aldrich, 0.78 g), and acetic acid (CH_3COOH, 99.7%, Samchun Chemicals, 10 ml) at room temperature. First, $BiVO_4$ films were spray-coated on indium tin oxide (ITO) substrates by the ESD process for 60 min. Fig. 1(a) shows a schematic of the ESD process for forming the $BiVO_4$ nanopillars; the process is described in detail in our previous reports [5,19]. Table 1 lists the conditions for the ESD process for producing the $BiVO_4$ films.

Table 1
Conditions for electrostatic spray deposition of the $BiVO_4$ film.

Items	Conditions
Substrate	Indium tin oxide (ITO) - coated glass
Applied voltage [kV]	8.5
ITO substrate dimensions [cm^2]	2.5 × 2.5
Distance nozzle to substrate [cm]	4.5
Coating time [min]	60
Substrate temperature, [$^{\circ}C$]	120
Annealing temperature [$^{\circ}C$]	550

2.2. Atomic layer deposition of ZnO and TiO_2 layers

Next, ZnO and TiO_2 layers were deposited onto the $BiVO_4$ nanopillar films, to create a heterojunction and improve the PEC performance. The ZnO and TiO_2 films were deposited by ALD (Lucida™ D series ALD system, NCDtech, Korea) using diethyl zinc (EGchem) and titanium (IV) isopropoxide (EGchem), respectively H_2O vapor was used as the oxidant. The conditions for the ALD fabrication of the ZnO and TiO_2 layers are listed in Table 2. The thickness of the ZnO layer was varied by changing the total number of cycles (n) at a deposition rate of 0.2 nm/cycle. Similarly, the thickness of the TiO_2 layer was controlled by changing the number of cycles at a deposition rate of 0.1 nm/cycle. We refer to the coatings as ZnO (n) and TiO_2 (n), with n indicating the number of cycles.

2.3. Film characterization

The structures of the various films were analyzed through X-ray diffraction (XRD) analysis (D/max-2500, Rigaku, Japan), which was performed using Cu Kα radiation for 2θ values of 20–65°. The compositional profiles of the films were obtained using Auger electron spectroscopy (AES, SAM 4300, Perkin Elmer). The depth profiles and surface chemical compositions of the films were obtained using X-ray photoelectron spectroscopy (XPS, X-TOOL, ULVAC-PHI). The morphologies of the $BiVO_4$ films were determined using high-resolution scanning electron microscopy (HR-SEM, XL30 SFEG, Phillips Co., Holland), which was performed at 15 kV. The morphology of ALD-coated $BiVO_4$ films was also characterized by transmission electron microscopy (TEM, JEM 2100F, JEOL Inc.). The TEM samples were prepared by the focused ion beam (FIB, 5 nA, LYRA3 XMH, TESCAN) technique to acquire a cross-sectional view.

2.4. Photoelectrochemical measurements

To observe the effects of the ZnO and TiO_2 coatings on $BiVO_4$, the water-splitting ability of the heterostructured film was evaluated based on its PCD. The $BiVO_4$ film was used as the working electrode while an Ag/AgCl electrode was employed as the reference electrode and a piece of Pt wire as the counter electrode. A 0.5 M Na_2SO_4 solution was used as the electrolyte. To simulate sunlight, we used a Xe arc lamp (Newport, Oriel Instruments, USA) equipped with an AM 1.5 filter. The current-voltage (I-V) characteristics were recorded using a potentiostat (VersaSTAT-3, Princeton Applied Research, USA) for applied voltages of 0.0–1.2 V (versus Ag/AgCl) at a scan rate of 10 mV/s. The incident photon-to-current efficiency (IPCE) was measured in a 0.5 M Na_2SO_4 solution (pH 7) using the same three-electrode system and a 300 W Xe lamp (Newport Oriel) with a CS 130 monochromator and a 10 nm slit. The output power was measured using a Si photodiode detector (Newport). Electrochemical impedance spectroscopy (EIS) measurements were performed using the aforementioned potentiostat (VersaSTAT-3, Princeton Applied Research, USA) and the same electrode configuration. The Nyquist plots were measured at 0.4 V (versus Ag/AgCl); a small sinusoidal perturbation (amplitude of 10 mV) was applied to the potential [20] over a frequency range of 100 kHz–100 mHz under dark and illuminated conditions. The measured spectra were fitted using the ZSimpWin program (VersaStudio).

Table 2
Conditions for ALD process.

Coatings	Overall pressure [Torr]	Process temperature [°C]	Deposition rate [nm/cycle]	Number of cycles
ZnO	3×10^{-1}	150	0.2	0, 50, 100,150,200,250
TiO_2	3×10^{-1}	200	0.1	0, 10,20,50,100,150

3. Results and discussion

3.1. Film characterization

In most previous studies on similar materials, the heterostructures investigated have been ITO/TiO_2/$BiVO_4$ and ITO/ZnO/$BiVO_4$. Here, we investigated the ITO/$BiVO_4$/ZnO/TiO_2 structure. Electrospray deposition, as employed here, requires a conductive substrate, and is thus well-suited for creating the nanostructured film directly on the conductive ITO substrate, but would not be effective for deposition on top of a low-conductivity ZnO or TiO_2 layer. Fig. 2(a) shows the XRD patterns of $BiVO_4$, $BiVO_4$/ ZnO 200, and $BiVO_4$/ ZnO 200/ TiO_2 100 films formed on ITO substrates. All samples exhibit clear diffraction peaks corresponding to the monoclinic crystal structure of $BiVO_4$ and the ITO substrate. The peaks related to monoclinic scheelite-like $BiVO_4$ observed at 2θ values of 29.0, 30.5, 34.6, 35.2, 39.9, 42.6, 45.4, 46.7, 50.3, 53.3, 58.5, and 59.2° correspond to the (1 2 1), (0 4 0), (2 0 0), (0 0 2), (2 1 1), (1 5 0), (2 3 1), (2 4 0), (2 0 2), (1 6 1), (3 2 1), and (1 2 3) planes, respectively [5,21]. Further, peaks related to ZnO can be seen at 31.9 and 34.1° while those related to TiO_2 appear at 28.6 and 36.1°. However, because the ZnO and TiO_2 layers were very thin, the intensities of these peaks were very low. Some of the peaks also overlap with those of $BiVO_4$.

Fig. 2(b) shows Raman spectra of the pristine $BiVO_4$ and heterostructured $BiVO_4$/ZnO/TiO_2 films. Peaks are visible at 129, 213, 326, 366, 718, and 827 cm^{-1}. The peaks at 129 and 213 cm^{-1} are assignable to the external (rotational/translational) modes of $BiVO_4$, while the peaks related to the $\delta_a(VO_4^{-3})$ and $\delta_{as}(VO_4^{-3})$ modes appear at approximately 326 and 366 cm^{-1}, respectively. These peaks correspond to the asymmetric and symmetric deformation modes of VO_4^{3-}. Further, peaks related to the asymmetric V-O stretching modes can be observed at 718 and 827 cm^{-1}; these are consistent with reference spectra[6,22–24]. The heterostructure $BiVO_4$/ZnO/TiO_2 film does not show any significant changes in the Raman spectra compared to the pristine film.

The compositional profile of the heterostructured film was investigated by AES, and the results are shown in Fig. 2(c). The figure shows the atomic concentration of each constituent element of the $BiVO_4$/ZnO/TiO_2 film as a function of the sputtering time. The concentration of Zn was approximately 16% at the surface and decreased to zero with an increase in the sputtering time. On the other hand, the concentrations of Bi and V were only 5% at the surface and increased to approximately 15–20% with an increase in the sputtering time, with their concentration ratio remaining almost constant. Thus, the AES results confirmed the successful synthesis of $BiVO_4$ in a 1:1 stoichiometric ratio. However, the concentration of Ti on the surface was very low compared to those of the other elements, owing to the lower thickness of the TiO_2 layer. In order to further confirm the formation of $BiVO_4$ nanopillars covered with ZnO and TiO_2, XPS depth profiling was performed. Fig. 2(d) shows the XPS spectra corresponding to the various constituent elements. Within the first 5 min of sputtering, a Zn2p peak and a Ti2p peak appear, confirming the presence of TiO_2 and ZnO on the surface. However, the Ti2p peak has a lower intensity due to the

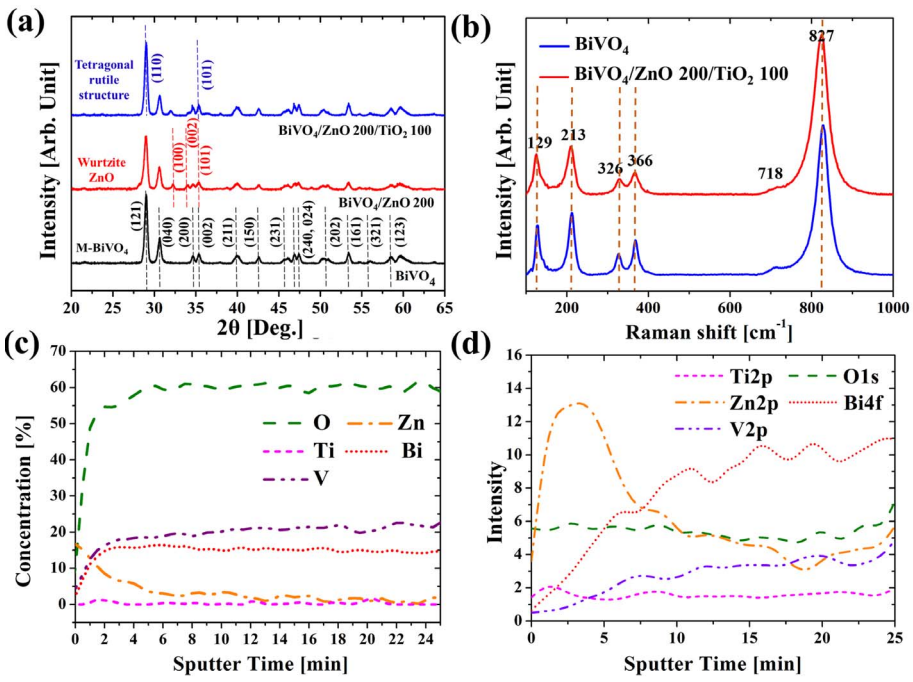

Fig. 2. (a) XRD patterns of $BiVO_4$, $BiVO_4$/ZnO 200, and $BiVO_4$/ZnO 200/TiO_2 100 (b) Raman spectra, and (c, d) depth profiles of $BiVO_4$/ZnO 200/TiO_2 100 film obtained by (c) AES and (d) XPS.

low thickness of the TiO_2 layer; in contrast, the thickness of the ZnO layer was significantly higher. On the other hand, the intensities of the Bi4f and V2p spectra at the surface are lower than those of the Zn2p and Ti2p spectra and increase with the sputtering time. Thus, the spectra in Fig. 2(d) confirmed that the ZnO and TiO_2 layers formed on the surface of the $BiVO_4$ coating were very thin.

The oxidation states of the constituent elements in the heterostructured film were also determined by XPS. Fig. 3(a) shows the Bi4f spectrum of the film. Two peaks are present at binding energies of 163.6 and 158.2 eV. These are the $Bi4f_{5/2}$ and $Bi4f_{7/2}$ peaks and can be attributed to Bi^{3+} in $BiVO_4$. These binding energies are typical for Bi in $BiVO_4$ [25,26]. Fig. 3(b) shows the V2p spectrum. $V2p_{3/2}$ and $V2p_{1/2}$ peaks can be seen at 515.7 and 522.2 eV, respectively. These XPS peaks, which are related to Bi^{3+} and V^{5+}, are consistent with the monoclinic scheelite-like phase of $BiVO_4$ [27–30]. Fig. 3(c) shows the Zn2p spectrum of the heterostructured film. $Zn2p_{1/2}$ and $Zn2p_{3/2}$ peaks are observed at 1044 and 1022 eV, respectively, indicating that Zn exists as Zn^{2+} in the film. Fig. 3(d) shows the Ti2p spectrum, which consists of two distinct peaks, at 458 and 464 eV; these are ascribable to $Ti2p_{3/2}$ and $Ti2p_{1/2}$ and have an energy difference of 6 eV. This energy gap in the Ti2p peaks indicates that Ti exists as Ti^{4+} in the film. Finally, the O1s and survey spectra are shown in Fig. 3(e) and Fig. 3(f), respectively. The O1s spectrum shows a peak at 529 eV, which is related to metal oxides

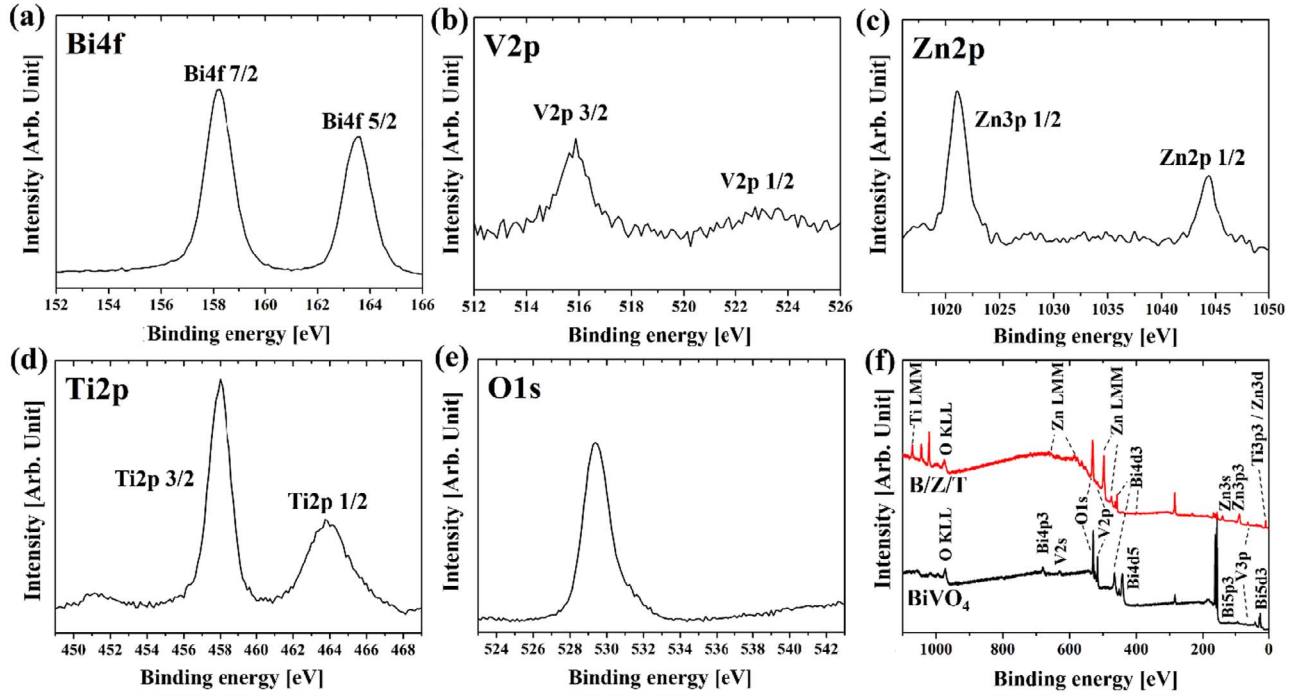

Fig. 3. High-resolution XPS spectra in the (a) Bi4f, (b) V2p, (c) Zn2p, (d) Ti2p, and (e) O1s energy ranges for $BiVO_4$/ZnO 200/TiO_2 100 film and (f) survey spectra of pristine $BiVO_4$ and heterostructured $BiVO_4$/ZnO 200/TiO_2 100 films.

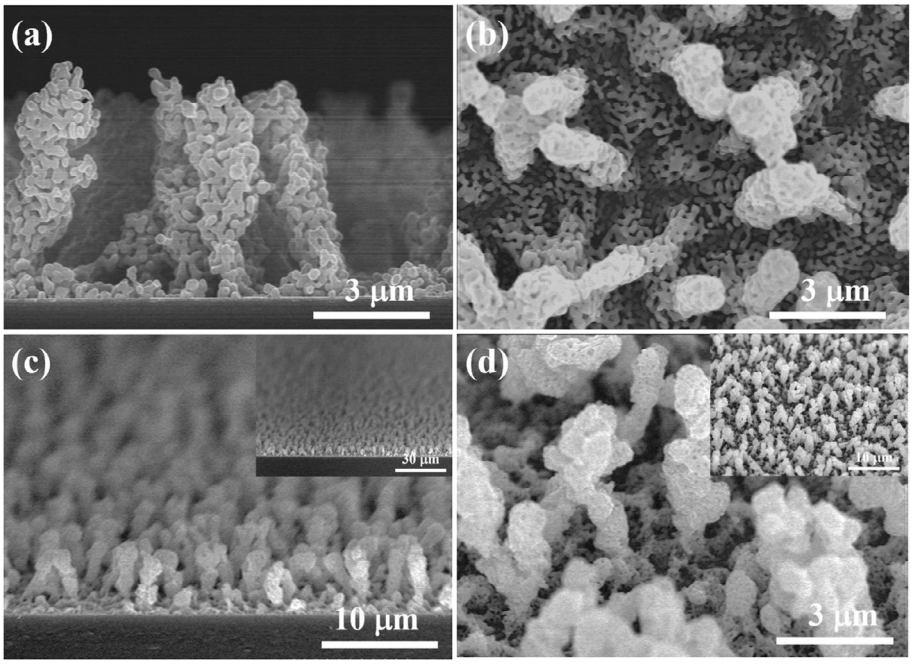

Fig. 4. SEM images of ALD-coated $BiVO_4$ film: (a) side view, (b) top view, (c) side-view tilted by 20°, and (d) top view tilted by 35°.

and confirms the presence of the oxides of Bi, V, Zn, and Ti [31,32]. Fig. 3 (f) shows the XPS survey spectra of the pristine $BiVO_4$ film and the $BiVO_4$/ZnO/TiO_2 film. The peaks related to Bi, V, O, Ti, and Zn confirm the presence of these elements in the fabricated heterostructure.

Next, the structures of the films were analyzed by SEM. Consistent with our previous reports for ESD-fabricated films, nanopillars of $BiVO_4$ were observed in the SEM images (Fig. 4). The formation of these structures through transport of the ESD droplets by simultaneous diffusion, thermophoresis, and electrophoresis is discussed in our prior study [5]. These nanopillars had a large surface area, which increases their effectiveness in water splitting, not only by providing more surface area on which PEC can occur, but by providing short charge-carrier transport distances to the surface. These effects produce a decrease in the rate of electron–hole recombination and an increase in the PCD [5,33]. As can be seen from Fig. 4(a, b), pillar-like structures about 5 μm in height were formed atop 300 to 500 nm thick films at the bottom. Each pillar consisted of a large number of nanosized $BiVO_4$ particles. Fig. 4(c, d) shows SEM images of the surface of a $BiVO_4$ film at tilt angles of 20 and, 35°, respectively. The insets in Fig. 4(c, d) shows forests of uniform $BiVO_4$ nanopillars covering the entire film area. These pillar-like structures are similar to villi (finger-like projections) and increase the surface area of the film. Thus, based on the images in Fig. 4, we conclude that the surface area of the $BiVO_4$ film was much higher than that of the underlying ITO film because of the pillar-like structures.

We also characterized the ALD-coated nanopillars at shorter length scale using transmission electron microscopy (TEM). The TEM image presented in Fig. 5(a–c) shows the nanoparticles making up part of a $BiVO_4$ pillar. The average size of the $BiVO_4$ nanoparticles is 140 ± 50 nm. Each nanoparticle is completely coated with ZnO and TiO_2. The $BiVO_4$ pillar was sectioned out of the film by FIB milling. The total thicknesses of the ZnO and TiO_2 around the $BiVO_4$ nanoparticle are ~25 and ~4 nm, respectively. The thickness of both films are lower than would be expected based on the nominal per-cycle ALD deposition rates, which are applicable to flat surfaces. The lowering of thickness is expected due to the high surface area of the porous pillar morphology of $BiVO_4$. Thus, with fixed precursor flow rate and number of cycles the full thickness expected for complete saturation of growth within each cycle was not obtained. The distribution of elements at the single nanoparticle level was measured using EDS elemental mapping as shown in Fig.5d. The thickness of ZnO is quite visible due to longer deposition time. However, the deposition rate and number of cycles during coating of TiO_2 are both lower, and a much thinner layer is produced.

3.2. Photoelectrochemical properties

The PCD values of the pristine and heterostructured $BiVO_4$ films in 0.5 M Na_2SO_4 as the electrolyte confirmed that the materials exhibited n-type characteristics. With respect to the photocatalytic splitting of water, the photocurrent observed under illumination is indicative of the amount of charge carriers generated by the incident photons and the degree to which they participate in water splitting. Here we used “back illumination”, which refers to illumination through the ITO-coated glass substrate. Therefore, higher-energy photons are absorbed nearer the ITO layer, whereas lower-energy photons are absorbed over a longer distance (and therefore on average further from the ITO layer). The PCD of the pristine $BiVO_4$ film was 0.9 mA/cm^2 at 1.2 V (versus Ag/AgCl), as represented by the solid line in Fig. 6(a); in contrast, the dark current for pristine $BiVO_4$ was almost zero. In this study, in order to improve the electrical and optical properties of $BiVO_4$, thin layers of ZnO and TiO_2 were formed on the $BiVO_4$ nanopillars by ALD. Further, the effects of the thicknesses of the ZnO and TiO_2 layers on the PEC performance of the heterostructured film were studied. Initially, the ZnO layer was deposited by ALD for 0, 50, 100, 150, 200 and 250 cycles, and then a layer of TiO_2 (100 cycles) was coated on top of the ZnO (Fig. 6(a)). In the absence of ZnO (ZnO 0), the PCD value improved slightly (1.1 mA/cm^2). With increasing thickness of the ZnO layer, the PCD increased further, reaching a maximum value (2.25 mA/cm^2) for 200 cycles of ZnO deposition. A further increase in the ZnO coating cycles to 250 resulted in a decrease in the PCD to 0.75 mA/cm^2. This may be due to an increase in the electron transport distance, which aided the recombination of charge carriers. The PCD value for the sample with 200 cycles of ZnO was 2.5 times higher than that for $BiVO_4$.

The PCD of the heterostructure films as a function of the thickness of the TiO_2 layer is shown in Fig. 6(b). For all the cases shown, the ZnO coating was fixed at 200 cycles. The maximum PCD value, 2.25 mA/cm^2, was achieved with a TiO_2 coating of 100 cycles. For TiO_2 coating greater than 100 cycles, the PCD dropped sharply, owing to a decrease in the charge-transfer efficiency. It has been reported previously that

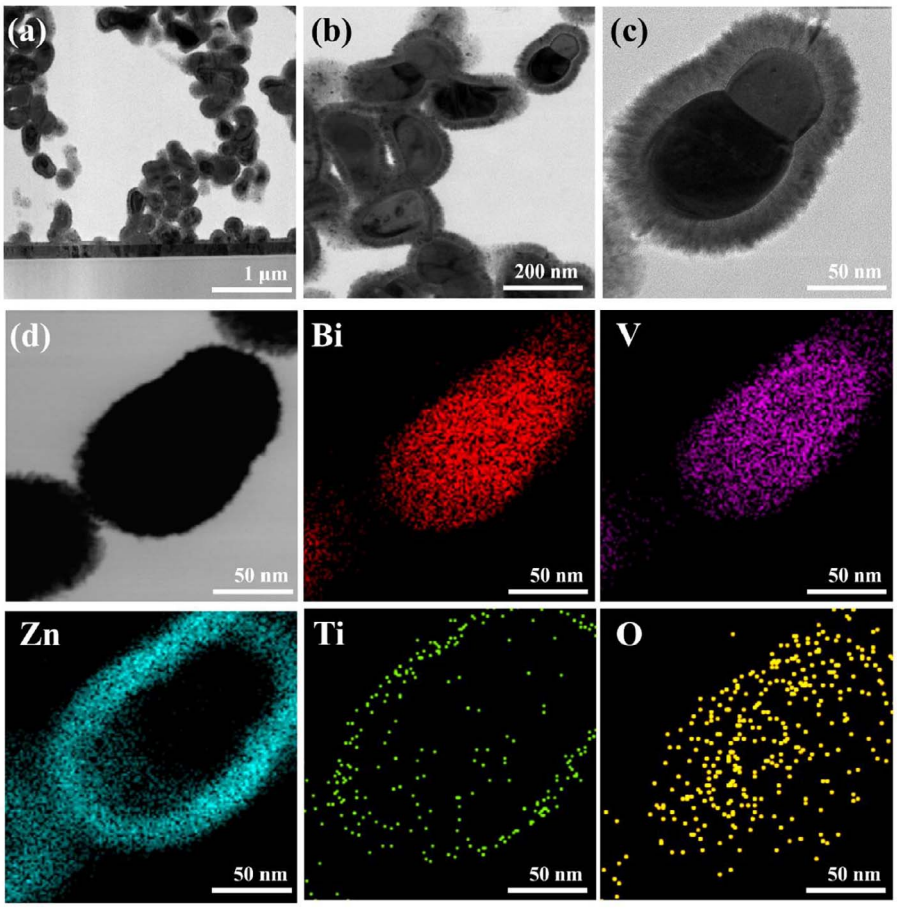

Fig. 5. TEM characterization of ALD-coated nanopillars. Panels (a), (b), and (c) show TEM images of $BiVO_4$/ZnO 200/TiO_2 100 nanostructures at different magnifications, while panel (d) shows the elemental mapping images centered on a single particle.

thin TiO_2 coatings improve the photocatalytic properties of similar heterostructures [14,34]. Thus, based on the above-described results, we conclude that the electrical and optical properties of $BiVO_4$ were enhanced by the ZnO and TiO_2 layers [35].

Fig. 6(c) shows IPCE curves of the $BiVO_4$ and $BiVO_4$/ZnO/TiO_2 films at 1.23 V (versus reversible hydrogen electrode (RHE)) as measured in 0.5 M Na_2SO_4 as the electrolyte. The IPCE value of the pristine $BiVO_4$ electrode was ~20% at 400 nm, with the photocurrent onset

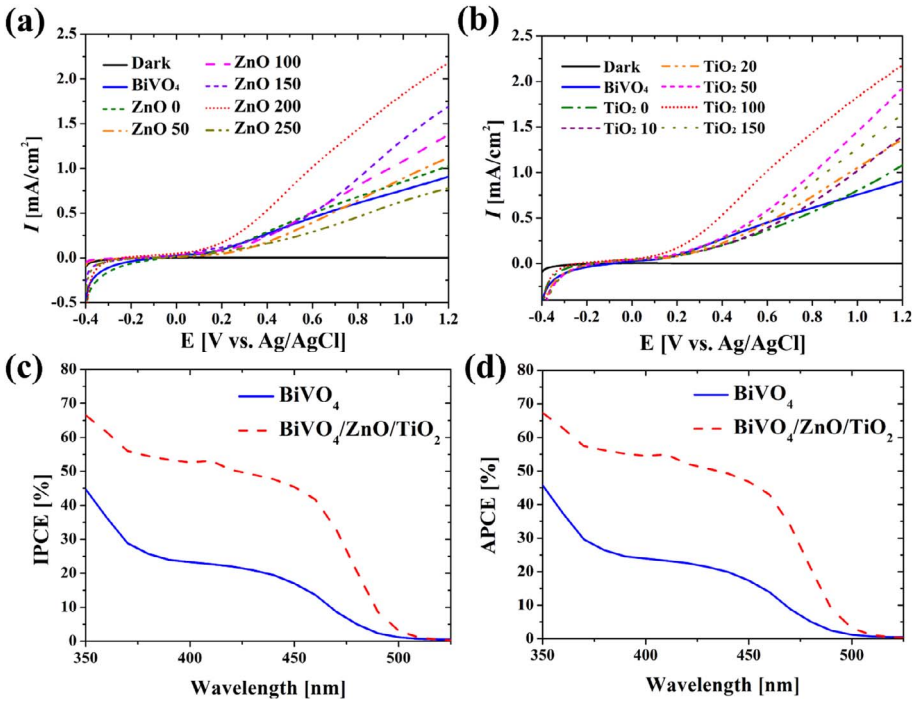

Fig. 6. PCD curves of $BiVO_4$/ZnO/TiO_2 heterostructure showing effects of (a) ZnO layer thickness and (b) TiO_2 layer thickness. (c) IPCE spectra and (d) APCE spectra of $BiVO_4$ and $BiVO_4$/ZnO200/TiO_2 100.

wavelength lying between 500 and 510 nm. This corresponds to a bandgap (E_g) of approximately 2.5 eV. On the other hand, the $BiVO_4$/ZnO/TiO_2 electrode showed a higher IPCE (53%) at 400 nm, with an onset wavelength similar to that of the pristine film. This confirmed that the heterostructured $BiVO_4$/ZnO/TiO_2 film-based electrode exhibited improved conversion efficiency and better light-harvesting properties mainly through improved charge separation, not increased absorbance. The IPCE of a photoactive material is dependent not only on charge separation efficiency, but also on losses arising from photons that are transmitted through the material or are reflected by it. To evaluate the inherent performance of the pristine $BiVO_4$ and heterostructured $BiVO_4$/ZnO/TiO_2 films, these losses should be excluded. For this purpose, we also determined the absorbed photon-to-current-efficiency (APCE), which is based only on the absorbed photons. The APCE is important for determining the optimal thickness for maximizing photon absorption and minimizing the transport distance for electron–hole pairs. The APCE can be expressed as the ratio of the IPCE and μ_{e^-/h^+}, where μ_{e^-/h^+} is the rate of electron–hole pair generation per unit incident photon flux.

$$\mathrm{APCE} = \mathrm{IPCE}/\mu_{e^-/h^+} \tag{1}$$

The absorbance was measured using a UV–visible spectrophotometer for wavelengths of 300–1000 nm. The APCE was then calculated from the IPCE and the absorbance (abs) using the following equation:

$$\mu_{e^-/h^+} = \frac{I_0 - I}{I_0} = 1 - \frac{I}{I_0} = 1 - 10^{-abs} \tag{2}$$

$$\mathrm{APCE}(\%) = \mathrm{IPCE}(\%)/[1 - 10^{-\mathrm{abs}}] \tag{3}$$

The APCE curves are similar to the IPCE, with the APCE values of the $BiVO_4$ and $BiVO_4$/ZnO/TiO_2 films being 24 and 55%, respectively, at 400 nm, as shown in Fig.6(d). However, the APCE value of the heterostructured $BiVO_4$/ZnO/TiO_2 film between wavelengths of 400–500 nm was significantly higher. The increased APCE indicates that the coating of the ZnO/TiO_2 layers improved electron–hole separation, in keeping with expectations. Further, the IPCE and APCE values were lower at longer wavelengths, probably owing to back illumination; the electrons generated at the surface have to travel a longer distance to reach the back contact. This increased transport length may result in a greater degree of trapping and recombination of the charge carriers, thus lowering the efficiency [36].

The EIS curves of the $BiVO_4$ and $BiVO_4$/ZnO/TiO_2 films as photoanode materials were measured in the dark and under simulated AM 1.5 sunlight conditions, to analyze their electron-diffusion and charge-transfer properties. Fig. 7 shows the impedance response during electrochemical impedance spectroscopy of the samples. The Randles equivalent circuit is shown in the inset; this circuit is a useful tool for analyzing the characteristic parameters. The resistances associated with the system, as indicated in the equivalent circuit, are the solution resistance (R_S), space-charge resistance (R_{SC}), and charge-transfer resistance (R_{CT}). Further, the space-charge capacitance (C_{SC}) within the semiconductor and the Helmholtz capacitance (C_H) at the electrolyte/electrode interface are also shown in the equivalent circuit along with the constant phase element (CPE). The values of these characteristic parameters are listed in Table 3. The Nyquist plots for the pristine $BiVO_4$ and heterostructured $BiVO_4$/ZnO/TiO_2 films shown in Fig. 7a and b indicate that the impedances of the $BiVO_4$ and $BiVO_4$/ZnO/TiO_2 samples were greater under dark conditions. This is attributable to the decrease in R_{SC} and R_{CT} under illumination. The heterostructure film exhibits a much smaller semicircle, owing to band bending, which lowers R_{SC} and R_{CT} and improves charge transfer. In addition, in the heterostructured film, the $BiVO_4$ layer is the primary light-absorbing layer, while the ZnO layer helps to confine the light (owing to its lower refractive index) within the $BiVO_4$ layer; this results in a decrease in the charge-transfer barrier at the interfaces formed by the ZnO layer. Therefore, the impedance of the heterostructured film under illumination is lower than that of the pristine $BiVO_4$ film under illumination and that of the heterostructured film under dark conditions. The values of the characteristic parameters are given in Table 3, which shows that the R_{CT} value (72 Ω) of the $BiVO_4$/ZnO/TiO_2 film is almost six times smaller than that of the $BiVO_4$ film (353 Ω) under illumination. Thus, the presence of the ZnO/TiO_2 layers on the $BiVO_4$ layer increased the charge-transfer rate, improved charge separation, and inhibited electron–hole pair recombination.

Table 3
Parameter values obtained from Randles equivalent circuit for $BiVO_4$ and $BiVO_4$/ZnO/TiO_2 films under dark and light conditions.

Parameters	$BiVO_4$		$BiVO_4$/ZnO/TiO_2	
	Dark	Light	Dark	Light
R_S (Ω)	63.3	63.7	48	47
C_{SC} (F)	6.6×10^{-4}	6.9×10^{-5}	5.6×10^{-6}	8.1×10^{-6}
R_{SC} (Ω)	422	388	153	22
C_H (F)	8.8×10^{-6}	1.1×10^{-5}	2.0×10^{-5}	3.8×10^{-5}
R_{CT} (Ω)	418	353	92	72
CPE (F)	3.73	3.5	3.23	2.8

The mechanism of photocurrent enhancement in the heterostructured film is illustrated in Fig. 8. The schematic of the mechanism shows the pillars of $BiVO_4$ on which ZnO and TiO_2 are conformally coated by ALD as described earlier. Under illumination, excited electrons and holes are generated mainly in the $BiVO_4$ layer and the electrons are rapidly conducted to the Pt electrode through the ITO layer, while holes go to the interface with the electrolyte. The rate of electron transfer is significantly lower in the dark. This is due to the overall series resistance of the four heterojunctions (ITO-$BiVO_4$, $BiVO_4$-ZnO, ZnO-TiO_2 and TiO_2-electrolyte) marked in Fig. 8 as J1, J2, J3 and J4 respectively. Because the conduction band energy (CB) of ZnO is more negative than that of $BiVO_4$, photo-generated electrons can move from the CB of ZnO to that of $BiVO_4$, but not in the other direction. In the

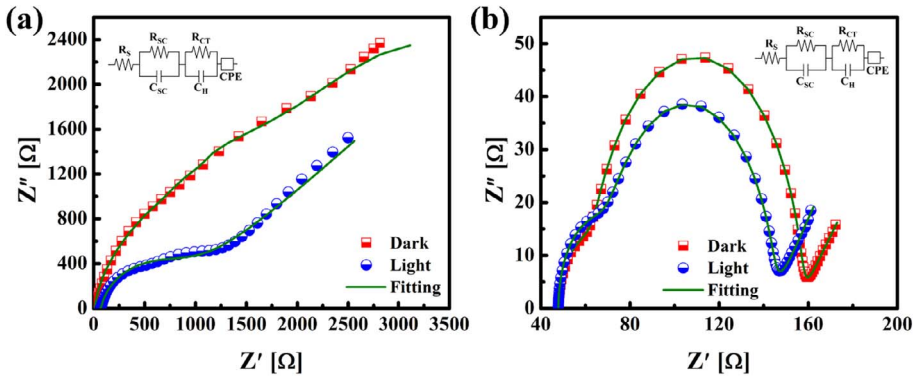

Fig. 7. Nyquist plots under dark and light conditions of (a) $BiVO_4$ and (b) $BiVO_4$/ZnO/TiO_2 films as photoanode materials. Insets show corresponding Randles equivalent circuits.

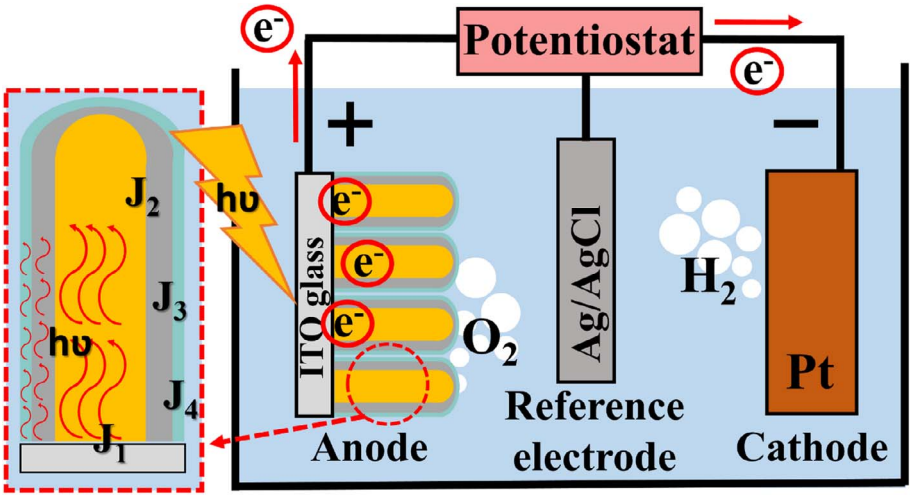

Fig. 8. The mechanism responsible for higher photocurrent in the heterostructured film.

Table 4
Comparison of PEC performances of $BiVO_4$ thin films fabricated in this study with those of similar films reported previously.

Materials	Reaction solution	PCD value at 1.23 V vs RHE[a], 1.20 V vs Ag/AgCl[b] [mA/cm^2]	Reference
$BiVO_4/TiO_2$	0.1 M NaOH	0.25[a]	[34]
ZnO/TiO_2	0.1 M NaOH	0.22[a]	[39]
$BiVO_4/ZnO$	0.5 M $NaClO_4$	0.60[b]	[16]
Co-Pi/$BiVO_4$/ZnO	0.2 M Na_2SO_4	1.95[b]	[12]
$BiVO_4/TiO_2$	0.1 M K_2PO_4	0.50[b]	[18]
$BiVO_4$/ZnO/TiO_2	**0.5 M Na_2SO_4**	**0.75[a]**	**Present**
$BiVO_4$/ZnO/TiO_2	**0.5 M Na_2SO_4**	**2.25[b]**	**Present**

presence of electrolyte and illumination, electrons from the ultra-thin TiO_2 layer can tunnel into the adjacent heterostructure layer (ZnO) as the Na_2SO_4 (electrolyte) introduces an electric field at electrode/electrolyte interface [37] Thus, TiO_2 contributes to photocurrent and provides holes at the TiO_2/electrolyte interface to drive oxygen evolution [38]. Application of a modest potential allows electrons to be transported from $BiVO_4/ZnO/TiO_2$ to ITO and holes to be driven to the TiO_2 surface where the water oxidation reaction occurs. The absorption of light at different wavelengths by the three semiconductor layers aids the generation of electron–hole pairs, as was evidenced by the APCE curves. Further, the TiO_2 layer over the ZnO layer results in the widening of the light-absorbance range and prevents surface corrosion during the PEC process [39]. Thus, the thickness-controlled heterostructured $BiVO_4/ZnO/TiO_2$ film exhibits better water-splitting capacity than that of the pristine $BiVO_4$ film.

Table 4 compares the PCD values obtained in this study with those for various previously reported heterojunctions of $BiVO_4$ with ZnO or TiO_2. Clearly, the use of a single layer, either of ZnO or TiO_2, with $BiVO_4$ does not result in the complete utilization of $BiVO_4$ for photocurrent generation. It should be noted that Moniz et al. observed similar values when they used a Co-Pi cocatalyst with a $ZnO/BiVO_4$ heterostructure. Thus, the performance of the heterostructured $BiVO_4/ZnO/TiO_2$ film, which exhibited a PCD of 2.25 mA/cm^2 at 1.2 V (versus Ag/AgCl (or ~0.8 mA/cm^2 at 1.23 V (versus RHE)) was superior to those reported previously. We conclude that the improved PCD was enabled by the ZnO/TiO_2 layers, which increased the charge-separation efficiency and passivated the surface of the $BiVO_4$ film, as evidenced by its improved stability.

4. Conclusions

We fabricated a heterostructured $BiVO_4/ZnO/TiO_2$ film by coating layers of ZnO and TiO_2 onto an electrospray deposited $BiVO_4$ porous nanopillar film, using atomic layer deposition. The heterostructured film consisting of ZnO (200 cycles) and TiO_2 (100 cycles) layers on the $BiVO_4$ layer exhibited a 2.25-fold increase in the PCD (2.5 mA/cm^2 at 1.2 V versus Ag/AgCl) compared to that of pristine $BiVO_4$. This enhancement is attributable to improved electron–hole pair separation and an increase in their lifetime because of the ZnO/TiO_2 layers. With respect to the ZnO/TiO_2 bilayer, the TiO_2 layer, owing to its low thickness, acts as a passivation layer while the ZnO layer contributes to electron–hole separation by forming a heterostructure with the $BiVO_4$ layer. The results presented here should aid the development of novel heterostructured electrode materials for photocatalysis and water splitting.

Acknowledgement

This research was supported by the Technology Development Program to Solve Climate Changes of the National Research Foundation (NRF) funded by the Ministry of Science, ICT & Future Planning (NRF-2016M1A2A2936760, NRF-2013M3A6B1078879, and NRF-2017R1A2B4005639) – Republic of Korea.

References

[1] A. Fujishima, Electrochemical photolysis of water at a semiconductor electrode, Nature 238 (1972) 37–38.
[2] P. Pookmanee, S. Kojinok, S. Phanichphant, Bismuth vanadate ($BiVO_4$) powder prepared by the sol-gel method, J. Met. Mater. Miner. 22 (2012) 49–53.
[3] S. Tokunaga, H. Kato, A. Kudo, Selective preparation of monoclinic and tetragonal $BiVO_4$ with scheelite structure and their photocatalytic properties, Chem. Mater. 13 (2001) 4624–4628.
[4] L. Chen, E. Alarcón-Lladó, M. Hettick, I.D. Sharp, Y. Lin, A. Javey, J.W. Ager, Reactive sputtering of bismuth vanadate photoanodes for solar water splitting, J. Phys. Chem. C 117 (2013) 21635–21642.
[5] H. Yoon, M.G. Mali, J.Y. Choi, M.-W. Kim, S.K. Choi, H. Park, S.S. Al-Deyab, M.T. Swihart, A.L. Yarin, S.S. Yoon, Nanotextured pillars of electrosprayed bismuth vanadate for efficient photoelectrochemical water splitting, Langmuir 31 (2015) 3727–3737.
[6] V. Merupo, S. Velumani, G. Oza, M. Makowska-Janusik, A. Kassiba, Structural, electronic and optical features of molybdenum-doped bismuth vanadium oxide, Mater. Sci. Semicond. Process. 31 (2015) 618–623.
[7] S. Xie, T. Zhai, Y. Zhu, W. Li, R. Qiu, Y. Tong, X. Lu, NiO decorated Mo: $BiVO_4$ photoanode with enhanced visible-light photoelectrochemical activity, Int. J. Hydrogen Energy 39 (2014) 4820–4827.
[8] B. Pattengale, J. Huang, The effect of Mo doping on the charge separation dynamics and photocurrent performance of $BiVO_4$ photoanodes, Phys. Chem. Chem. Phys. 18

(2016) 32820–32825.
[9] D.K. Zhong, S. Choi, D.R. Gamelin, Near-complete suppression of surface recombination in solar photoelectrolysis by "Co-Pi" catalyst-modified W: $BiVO_4$, J. Am. Chem. Soc. 133 (2011) 18370–18377.
[10] H. Jung, S.Y. Chae, C. Shin, B.K. Min, O.-S. Joo, Y.J. Hwang, Effect of the Si/TiO_2/$BiVO_4$ heterojunction on the onset potential of photocurrents for solar water oxidation, ACS Appl. Mater. Interfaces 7 (2015) 5788–5796.
[11] J. Su, L. Guo, N. Bao, C.A. Grimes, Nanostructured WO_3/$BiVO_4$ heterojunction films for efficient photoelectrochemical water splitting, Nano Lett. 11 (2011) 1928–1933.
[12] S.J. Moniz, J. Zhu, J. Tang, 1D Co-Pi Modified $BiVO_4$/ZnO junction cascade for efficient photoelectrochemical water cleavage, Adv. Energy Mater. 4 (2014) 1301590.
[13] A.P. Singh, N. Kodan, B.R. Mehta, A. Held, L. Mayrhofer, M. Moseler, Band edge engineering in $BiVO_4$/TiO_2 heterostructure: enhanced photoelectrochemical performance through improved charge transfer, ACS Catal. 6 (2016) 5311–5318.
[14] A.G. Scheuermann, J.D. Prange, M. Gunji, C.E. Chidsey, P.C. McIntyre, Effects of catalyst material and atomic layer deposited TiO_2 oxide thickness on the water oxidation performance of metal–insulator–silicon anodes, Energ. Environ. Sci. 6 (2013) 2487–2496.
[15] S. Hu, M.R. Shaner, J.A. Beardslee, M. Lichterman, B.S. Brunschwig, N.S. Lewis, Amorphous TiO_2 coatings stabilize Si GaAs, and GaP photoanodes for efficient water oxidation, Science 344 (2014) 1005–1009.
[16] X. Fu, M. Xie, P. Luan, L. Jing, Effective visible-excited charge separation in silicate-bridged ZnO/$BiVO_4$ nanocomposite and its contribution to enhanced photocatalytic activity, ACS Appl. Mater. Interfaces 6 (2014) 18550–18557.
[17] S. Balachandran, N. Prakash, K. Thirumalai, M. Muruganandham, M. Sillanpää, M. Swaminathan, Facile construction of heterostructured $BiVO_4$–ZnO and its dual application of greater solar photocatalytic activity and self-cleaning property, Ind. Eng. Chem. Res. 53 (2014) 8346–8356.
[18] S. Ho-Kimura, S.J. Moniz, A.D. Handoko, J. Tang, Enhanced photoelectrochemical water splitting by nanostructured $BiVO_4$–TiO_2 composite electrodes, J. Mater. Chem. A 2 (2014) 3948–3953.
[19] H. Yoon, J.H. Woo, Y.M. Ra, S.S. Yoon, H.Y. Kim, S. Ahn, J.H. Yun, J. Gwak, K. Yoon, S.C. James, Electrostatic spray deposition of copper–indium thin films, Aerosol Sci. Technol. 45 (2011) 1448–1455.
[20] T. Lopes, L. Andrade, F. Le Formal, M. Gratzel, K. Sivula, A. Mendes, Hematite photoelectrodes for water splitting: evaluation of the role of film thickness by impedance spectroscopy, Phys. Chem. Chem. Phys. 16 (2014) 16515–16523.
[21] W. Yin, W. Wang, M. Shang, L. Zhou, S. Sun, L. Wang, $BiVO_4$ hollow nanospheres: anchoring synthesis, growth mechanism, and their application in photocatalysis, Eur. J. Inorg. Chem. 2009 (2009) 4379–4384.
[22] A. Kudo, Development of photocatalyst materials for water splitting, Int. J. Hydrogen Energy 31 (2006) 197–202.
[23] L. Ren, L. Jin, J.-B. Wang, F. Yang, M.-Q. Qiu, Y. Yu, Template-free synthesis of $BiVO_4$ nanostructures: i nanotubes with hexagonal cross sections by oriented attachment and their photocatalytic property for water splitting under visible light, Nanotechnology 20 (2009) 115603.
[24] P. Brack, J.S. Sagu, T. Peiris, A. McInnes, M. Senili, K. Wijayantha, F. Marken, E. Selli, Aerosol-Assisted CVD of Bismuth Vanadate Thin Films and Their Photoelectrochemical Properties, Chem. Vap. Deposition 21 (2015) 41–45.
[25] M. Zalfani, B. van der Schueren, Z.-Y. Hu, J.C. Rooke, R. Bourguiga, M. Wu, Y. Li, G. Van Tendeloo, B.-L. Su, Novel 3DOM $BiVO_4$/TiO_2 nanocomposites for highly enhanced photocatalytic activity, J. Mater. Chem. A 3 (2015) 21244–21256.
[26] X. Zhang, B. Zhang, K. Cao, J. Brillet, J. Chen, M. Wang, Y. Shen, A perovskite solar cell-TiO_2@$BiVO_4$ photoelectrochemical system for direct solar water splitting, J. Mater. Chem. A 3 (2015) 21630–21636.
[27] K.P.S. Parmar, H.J. Kang, A. Bist, P. Dua, J.S. Jang, J.S. Lee, Photocatalytic and Photoelectrochemical Water Oxidation over Metal-Doped Monoclinic $BiVO_4$ Photoanodes, ChemSusChem 5 (2012) 1926–1934.
[28] A.Y. Booshehri, S.C.-K. Goh, J. Hong, R. Jiang, R. Xu, Effect of depositing silver nanoparticles on $BiVO_4$ in enhancing visible light photocatalytic inactivation of bacteria in water, J. Mater. Chem. A 2 (2014) 6209–6217.
[29] H. Li, Y. Sun, B. Cai, S. Gan, D. Han, L. Niu, T. Wu, Hierarchically Z-scheme photocatalyst of Ag@ AgCl decorated on $BiVO_4$ (040) with enhancing photoelectrochemical and photocatalytic performance, Appl. Catal. B: Environ. 170 (2015) 206–214.
[30] C.M. Ghimbeu, E. Raymundo-Piñero, P. Fioux, F. Béguin, C. Vix-Guterl, Vanadium nitride/carbon nanotube nanocomposites as electrodes for supercapacitors, J. Mater. Chem. 21 (2011) 13268–13275.
[31] D.R. Kumar, D. Manoj, J. Santhanalakshmi, Au–ZnO bullet-like heterodimer nanoparticles: synthesis and use for enhanced nonenzymatic electrochemical determination of glucose, RSC Adv. 4 (2014) 8943–8952.
[32] F. Dong, X. Feng, Y. Zhang, C. Gao, Z. Wu, An anion-exchange strategy for 3D hierarchical $(BiO)_2CO_3$/amorphous Bi_2S_3 heterostructures with increased solar absorption and enhanced visible light photocatalysis, RSC Adv. 5 (2015) 11714–11723.
[33] T.W. Kim, K.-S. Choi, Nanoporous $BiVO_4$ photoanodes with dual-layer oxygen evolution catalysts for solar water splitting, Science 343 (2014) 990–994.
[34] M. Xie, X. Fu, L. Jing, P. Luan, Y. Feng, H. Fu, Long-lived, visible-light-excited charge carriers of TiO_2/$BiVO_4$ nanocomposites and their unexpected photoactivity for water splitting, Adv. Energy Mater. 4 (2014) 1300995.
[35] R. Hussin, K.-L. Choy, X. Hou, Enhancement of crystallinity and optical properties of bilayer TiO_2/ZnO thin films prepared by atomic layer deposition, J. Nanosci. Nanotechnol. 11 (2011) 8143–8147.
[36] A. Fillinger, B. Parkinson, The adsorption behavior of a ruthenium-based sensitizing dye to nanocrystalline TiO_2 coverage effects on the external and internal sensitization quantum yields, J. Electrochem. Soc. 146 (1999) 4559–4564.
[37] R. van de Krol, Y. Liang, J. Schoonman, Solar hydrogen production with nanostructured metal oxides, J. Mater. Chem. 18 (2008) 2311–2320.
[38] Y. Vidya, B. Lakshminarasappa, Synthesis, characterization and thermoluminescence studies of $LiNaSO_4$: Eu_3^+ nanophosphor, J. Lumin. Appl. 1 (2014) 40–60.
[39] S. Hernández, V. Cauda, A. Chiodoni, S. Dallorto, A. Sacco, D. Hidalgo, E. Celasco, C.F. Pirri, Optimization of 1D ZnO@ TiO_2 core–shell nanostructures for enhanced photoelectrochemical water splitting under solar light illumination, ACS Appl. Mater. Interfaces 6 (2014) 12153–12167.